Available online at www.sciencedirect.com
SCIENCE DIRECT®
Journal of Magnetic Resonance 168 (2004) 137–146
JMR Journal of Magnetic Resonance
www.elsevier.com/locate/jmr

Rotational resonance in uniformly ^{13}C-labeled solids: effects on high-resolution magic-angle spinning NMR spectra and applications in structural studies of biomolecular systems

Aneta T. Petkova and Robert Tycko*

Laboratory of Chemical Physics, National Institute of Diabetes and Digestive and Kidney Diseases, National Institutes of Health, Bethesda, MD 20892-0520, USA

Received 8 October 2003; revised 30 January 2004

Abstract

We describe investigations of the effects of rotational resonance (R^2) on solid state ^{13}C NMR spectra of uniformly ^{13}C-labeled samples obtained under magic-angle spinning (MAS), and of the utility of R^2 measurements as structural probes of peptides and proteins with multiple uniformly labeled residues. We report results for uniformly ^{13}C-labeled L-alanine and L-valine in polycrystalline form, and for amyloid fibrils formed by the 15-residue peptide Aβ_{11-25} with uniform labeling of a four-residue segment. The MAS NMR spectra reveal a novel *J*-decoupling effect at R^2 conditions that may be useful in spectral assignments for systems with sharp ^{13}C MAS NMR lines. Pronounced dependences of the apparent isotropic ^{13}C NMR chemical shifts on MAS frequency near R^2 conditions are also observed. We demonstrate the feasibility of quantitative ^{13}C–^{13}C distance determinations in L-valine, and qualitative determinations of inter-residue ^{13}C–^{13}C contacts in Aβ_{11-25} fibrils. Finally, we demonstrate a "relayed" R^2 technique that may be useful in structural measurements on systems with poorly resolved ^{13}C MAS NMR lines.
Published by Elsevier Inc.

Keywords: Solid state NMR; Magic-angle spinning; Rotational resonance; Amyloid structure

1. Introduction

Recent solid state nuclear magnetic resonance (NMR) studies of a variety of systems [1–10] have demonstrated the feasibility and utility of two-dimensional (2D) ^{13}C–^{13}C and ^{15}N–^{13}C spectroscopy of peptides and proteins with uniformly ^{15}N- and ^{13}C-labeled amino acid residues. Measurements of chemical shifts and linewidths in the 2D spectra provide valuable constraints on secondary structure and structural order [3,4,11,12]. Quantitative or approximate measurements of internuclear distances in samples with uniformly labeled residues would provide additional constraints on tertiary and quaternary structure, sidechain conformations, and sidechain–sidechain contacts that would contribute greatly to the determination of complete molecular and supramolecular structures. In magic-angle spinning (MAS) NMR studies of selectively isotopically labeled samples, dipolar recoupling techniques are frequently used for internuclear distance measurements. In studies of uniformly labeled samples, dipolar recoupling techniques that are not frequency-selective generally lead to coupled, multiple-spin systems whose dynamics are dominated by the shortest (e.g., one-bond) internuclear distances. Non-selective dipolar recoupling techniques are therefore of limited value as sources of distance constraints in uniformly labeled systems.

The rotational resonance (R^2) effect, originally described by Andrew et al. [13] and subsequently developed as a structural tool [14–20], provides a means of recoupling pairs of ^{13}C nuclei whose isotropic chemical shift difference equals the MAS frequency ν_R or a multiple thereof. Quite recently, Williamson et al. [21] have shown that ^{13}C R^2 measurements on uniformly labeled compounds can be carried out and interpreted in terms of pairwise ^{13}C–^{13}C distances, provided that the one-dimensional (1D) ^{13}C MAS NMR spectrum is

* Corresponding author. Fax: 1-301-496-0825.
E-mail address: tycko@helix.nih.gov (R. Tycko).

1090-7807/$ - see front matter. Published by Elsevier Inc.
doi:10.1016/j.jmr.2004.02.007

sufficiently well resolved that only two inequivalent ^{13}C-labeled sites are on or close to R^2 at a time. Williamson et al. presented and analyzed experimental R^2 polarization transfer curves for uniformly labeled L-threonine in polycrystalline powder form. In related earlier work, Terao and co-workers [22] demonstrated the applicability of "rotational resonance in the tilted rotating frame" to distance measurements in uniformly ^{13}C-labeled peptides. Dusold et al. [23] have analyzed ^{13}C MAS NMR spectra of a uniformly ^{13}C-labeled compound at R^2 conditions. Duma et al. [24] have analyzed ^{13}C lineshapes in uniformly labeled L-alanine near R^2 conditions. Samoson et al. [25] have described 2D ^{13}C–^{13}C spectra of uniformly labeled systems in which crosspeaks are generated by sweeping the MAS frequency through R^2 conditions.

In this paper, we report the results of additional R^2 measurements on uniformly labeled systems, including two polycrystalline amino acids (U-^{15}N, ^{13}C-L-alanine and U-^{15}N, ^{13}C-L-valine, referred to below as U-Ala and U-Val) and non-crystalline amyloid fibrils formed by the synthetic peptide Aβ_{11-25} (residues 11–25 of the 40-residue Alzheimer's β-amyloid peptide), with uniform labeling of residues 18–21 (referred to below as VFFA-Aβ_{11-25}). These data provide further evidence for the effectiveness of R^2 measurements on uniformly labeled systems. We demonstrate significant dependences of apparent ^{13}C chemical shifts on MAS frequencies in the vicinity of R^2 conditions, previously described by others [15,20,24,26,27], which should be considered when ^{13}C chemical shift assignments are extracted from 2D or higher-dimensional MAS spectra of uniformly labeled samples, and a novel *J*-decoupling effect that occurs in R^2 measurements on systems of three or more coupled ^{13}C nuclei. Finally, we discuss and demonstrate a "relayed" R^2 technique that may be particularly useful in R^2 measurements on systems with unresolved or poorly resolved ^{13}C MAS NMR lines.

2. Materials and methods

Uniformly labeled amino acids were obtained from Cambridge Isotopes Laboratory. U-Ala was used as received. U-Val was recrystallized from water. The VFFA-Aβ_{11-25} peptide (residues 11–25 of the 40-residue β-amyloid peptide associated with Alzheimer's disease [4,28], amino acid sequence EVHHQKLVFFAEDVG) was prepared by standard solid phase synthesis methods, using *N*-fluorenylmethoxycarbonyl (FMOC) chemistry. FMOC-protected, uniformly labeled L-valine, L-phenylalanine, and L-alanine were incorporated at the V18, F19, F20, and A21 positions (with residue numbers based on the full-length β-amyloid sequence), while all other residues were not labeled. Reverse phase high-performance liquid chromatography (Vydac preparative C18 column) yielded >95% pure peptide, as verified by electrospray mass spectrometry. Fibrils were grown by incubation of a 10 mM peptide solution at, pH 7.4, for 21 days, and lyophilized for the solid state NMR experiments. Transmission electron microscope images of negatively stained fibrils, X-ray powder diffraction, and a variety of solid state NMR experiments indicate the formation of amyloid fibrils with an extended antiparallel β-sheet structure [28].

All NMR experiments were performed at a ^{13}C NMR frequency of 150.7 MHz, using a Varian Infinity spectrometer console and a 3.2 mm Varian T3 MAS probe. Fig. 1 shows the radio-frequency (RF) pulse sequences used in our experiments. For 1D spectra, ^{13}C magnetization was created with ramped cross polarization (CP) from ^{1}H under MAS (Fig. 1A). For R^2 measurements,

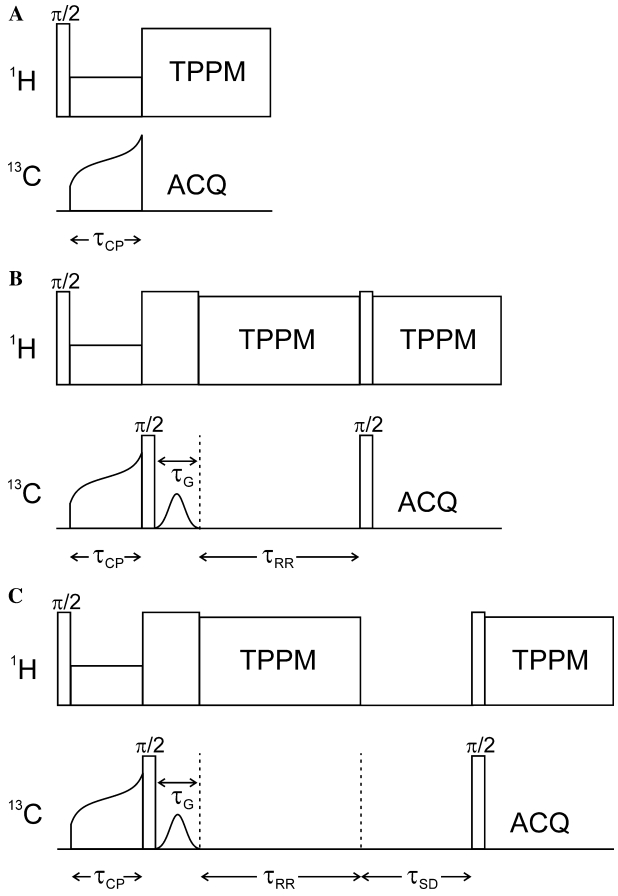

Fig. 1. Radio-frequency pulse sequences for rotational resonance experiments under MAS. (A) Sequence for measurement of cross-polarized ^{13}C NMR spectra, with tangent-function modulation of the ^{13}C RF amplitude during the cross polarization period τ_{CP}, and with TPPM decoupling during signal acquisition (ACQ). (B) Sequence for ^{13}C polarization transfer measurements. One or more ^{13}C lines are inverted by a Gaussian-shaped π pulse of length τ_G. Difference spectra may be recorded by placing the RF carrier frequency during τ_G either on-resonance or far off-resonance with these lines. Polarization transfer to other lines occurs during the rotational resonance period τ_{RR}. (C) Sequence for relayed rotational resonance. ^{13}C–^{13}C spin diffusion during τ_{SD} occurs in the absence of proton decoupling.

the ^{13}C magnetization was rotated to the $+z$ axis after CP, and the resonance of interest was selectively inverted (to $-z$) with a weak Gaussian-shaped pulse (1.0 ms duration). After the R^2 mixing period τ_{RR}, the ^{13}C magnetization was rotated back to the xy plane and free-induction decay (FID) signals were acquired (Fig. 1B). In relayed R^2 measurements, an additional period τ_{SD} of ^{13}C polarization transfer via proton-driven spin diffusion was applied after τ_{RR} (Fig. 1C). Relayed R^2 data reported below were obtained with no RF fields during τ_{SD}. Relayed R^2 experiments carried out with a proton RF field amplitude equal to ν_R during τ_{SD}, to enhance ^1H–^1H and ^1H–^{13}C dipole–dipole couplings [29], gave similar results. Proton decoupling levels were 100 kHz, with two-pulse phase modulation (TPPM) [30] during τ_{RR} and signal acquisition. MAS frequencies were stabilized to within 3 Hz of the nominal values. Unless otherwise indicated, R^2 conditions discussed below and in figure captions are the $n = 1$ conditions, where ν_R equals the difference between isotropic chemical shift frequencies of two ^{13}C NMR lines of interest.

Simulations of R^2 polarization transfer curves were carried out with a Fortran program written specifically for this purpose. Using a density matrix formalism, the program calculates the evolution of a two-spin system under MAS, including the time-dependent dipole–dipole coupling, isotropic chemical shifts, and time-dependent chemical shift anisotropies (CSA), and assuming an initial condition in which spin polarization resides on only one of the two ^{13}C spins. CSA principal values were set to be negligibly small in simulations presented below, as the CSA has only minor effects on $n = 1$ R^2 polarization transfer. Simulated curves were averaged over 1728 crystallite orientations. A time step $\delta t = 24/\nu_R$ was used in all simulations. Effects of transverse spin relaxation were included by multiplying all density matrix elements ρ_{ij} by factors $\exp[-(|\Delta m_{ij}^{(1)}| + |\Delta m_{ij}^{(2)}|)\delta t/T_2]$ after each time step, where $\Delta m_{ij}^{(k)}$ is the change in z-component of angular momentum for spin k associated with ρ_{ij}. The average transverse relaxation rate is given by $1/T_2 = (1/T_2^{(1)} + 1/T_2^{(2)})/2$, where $T_2^{(1)}$ and $T_2^{(2)}$ are single-quantum transverse relaxation times for the two coupled spins, determined from experimental spin-echo measurements performed with TPPM decoupling and at MAS frequencies far from R^2 conditions. This use of an average transverse relaxation rate is justified by the usual assumption that transverse relaxation results from uncorrelated random fields at the two ^{13}C sites. Incorporation of transverse relaxation into density matrix simulations as a simple exponential damping of coherences is equivalent to a full Liouvillian treatment of transverse relaxation in this case, because only one coherence and one relaxation rate would enter into such a treatment of polarization transfer in an ideal two-spin system and in the absence of RF pulses and longitudinal relaxation [31]. Measurement of $T_2^{(1)}$ and $T_2^{(2)}$ far from R^2 conditions is necessary to prevent mixing of the transverse relaxation rates of coupled spins near R^2.

The damping of R^2 polarization transfer curves calculated as described above is in reasonable agreement with the explicitly stochastic treatment of Williamson et al. [21], in which fluctuating isotropic shifts were introduced to simulate relaxation processes. The validity of our treatment of spin relaxation is also supported empirically by data presented below.

3. Results and discussion

3.1. Effects of rotational resonance on 1D spectra

Fig. 2 shows 1D ^{13}C CP/MAS NMR spectra of U-Ala at selected values of ν_R. Spectra for which the R^2 condition is fulfilled between the CO and Cβ lines and

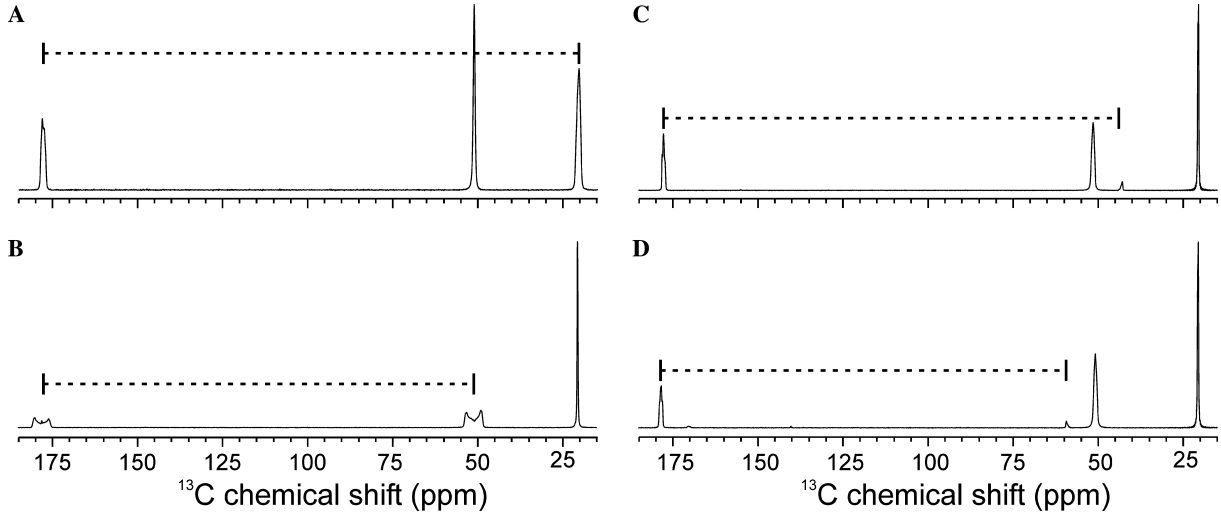

Fig. 2. ^{13}C NMR spectra of U-Ala at rotational resonance between the CO and Cβ lines (A), at rotational resonance between the CO and Cα lines (B), and near rotational resonance between the CO and Cα lines (C and D). Dashed lines indicate the MAS frequencies as offsets from the CO line.

between the CO and Cα lines are shown in Figs. 2A and B, respectively. The lineshapes of the peaks under R^2 reflect the dipole–dipole coupling between the spins. Spectra in Figs. 2C and D were obtained with ν_R either 1.11 kHz above or 1.11 kHz below the R^2 condition between the CO and Cα lines, and already show significant broadening of the two lines. Fig. 3 shows aliphatic regions of 1D CP/MAS spectra of U-Val at selected values of ν_R. Due to the presence of two inequivalent molecules in the crystalline unit cell of L-valine with different sidechain torsion angles [32], two partially resolved NMR lines are observed for the Cβ, Cγ1, and Cγ2 sites. The two lines are best resolved for Cγ1 (the less shielded Cγ resonance), for which splittings due to the Cβ–Cγ1 J couplings are observed. In order to illustrate R^2 effects in U-Val, spectra with ν_R values that produce recoupling between the CO carbon and the Cγ2 (Fig. 3A), Cβ (Fig. 3B), and Cα (Fig. 3C for $n = 1$; Fig. 3D for $n = 2$) carbons are presented. ^{13}C NMR lines under R^2 show the expected broadenings due to the unsuppressed dipole–dipole couplings.

The spectra in Figs. 2 and 3 illustrate two interesting effects. First, R^2 between the CO carbon and one of the aliphatic carbons appears to remove J couplings to other aliphatic carbons, producing a *narrowing* of the ^{13}C MAS NMR lines of sites that are not on R^2. This effect is most clearly seen in Fig. 3B, where the R^2 condition between the CO and Cβ carbons of U-Val causes the disappearance of the J splittings of the Cγ1 lines. The same J-decoupling effect, resulting in line narrowing, can also be seen for the Cγ2 (Fig. 3B), and Cβ (Figs. 3A, C, and D) lines. J-decoupling due to R^2 may be useful as a means of assigning ^{13}C lines in MAS spectra of uniformly labeled compounds (provided the intrinsic linewidths are sufficiently small that effects of J couplings are observable), or as a means of eliminating ambiguities in the structural interpretation of R^2 data arising from poor spectral resolution (see below). This J-decoupling effect is attributable mathematically to the fact that ^{13}C–^{13}C J couplings do not commute with the effective ^{13}C–^{13}C dipole–dipole coupling at an R^2 condition. Second, shifts of the apparent ^{13}C NMR frequencies occur as ν_R is varied from below R^2 to above R^2. These shifts are most apparent for the most strongly coupled ^{13}C pairs, e.g., the CO–Cα pairs. As seen in Figs. 2C and D and 3E and F, the Cα line is shifted upfield when ν_R is below the CO–Cα R^2 condition and downfield when ν_R is above this condition. The CO line exhibits the opposite shifts. Apparent shifts of ^{13}C NMR lines near R^2 conditions have been reported and discussed in earlier studies [15,20,24,26,27]. These shifts should be taken into account in measurements and analyses of ^{13}C chemical shifts in 1D or multidimensional ^{13}C MAS spectra, and in comparisons of spectra obtained at different ν_R values.

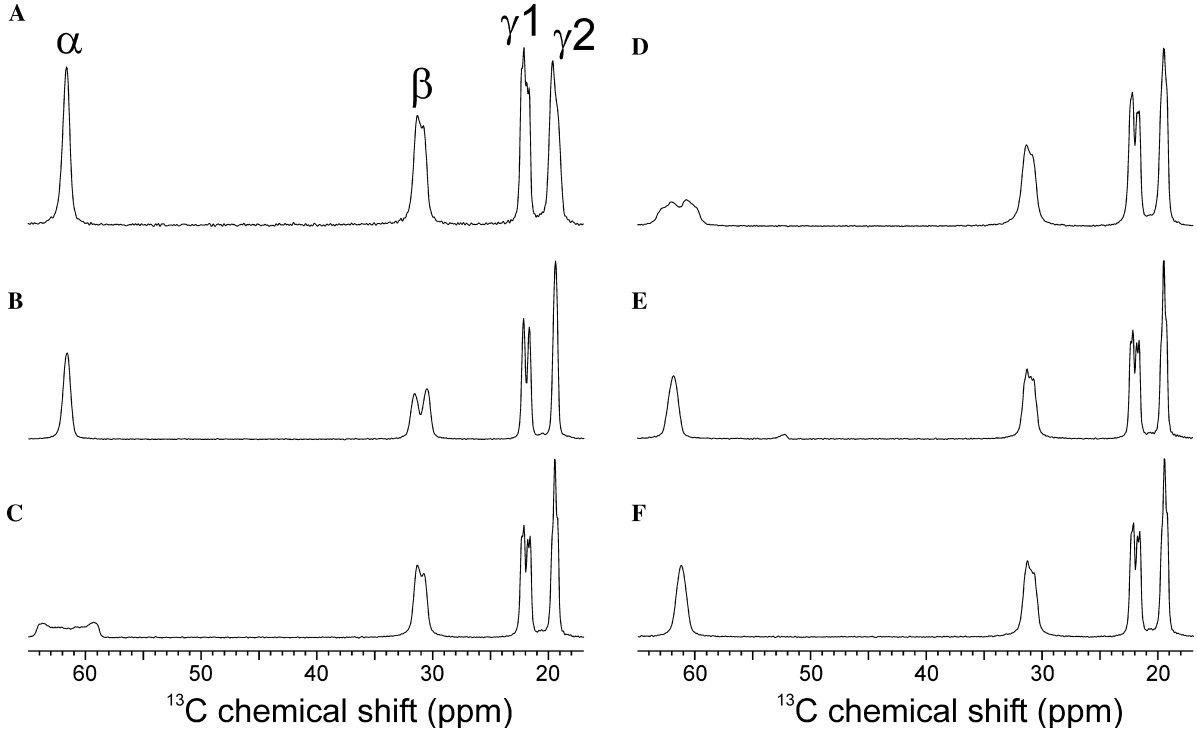

Fig. 3. Aliphatic regions of ^{13}C NMR spectra of U-Val at rotational resonance between the CO and Cγ2 lines (A), at rotational resonance between the CO and Cβ lines (B), at rotational resonance between the CO and Cα lines (C and D), 8.6 ppm above rotational resonance between the CO and Cα lines (E), and 8.6 ppm below rotational resonance between the CO and Cα lines (F). Spectrum (D) is at the $n = 2$ rotational resonance condition.

In order to characterize more fully the R^2 effects on 1D ^{13}C CP/MAS spectra of uniformly labeled compounds, we have acquired series of spectra with ν_R varying from 24.0 to 17.9 kHz (U-Ala) and from 23.8 to 7.9 kHz (U-Val) in steps of 30 Hz. Peak fitting with a single Gaussian line for the U-Ala Cβ and the U-Val CO was performed within the Varian Spinsight software. Fig. 4A shows a plot of the apparent linewidth of the U-Ala Cβ peak as ν_R is lowered to pass through the R^2 condition between the CO and Cβ lines, and then between the CO and Cα lines. The linewidth shows a continuous change from 70 to 190 Hz and back over a ν_R range of roughly 600 Hz around the R^2 condition between CO and Cβ, and a further reduction as the first CO spinning sideband moves towards the Cα line. Tracking the CO and Cα line broadening profiles as they pass through R^2, the Cβ line goes through a partial *J*-decoupling from 61 to 47 Hz and back to 61 Hz over a range of 2.2 kHz. Fig. 4B shows the dependence of the apparent CO chemical shift on ν_R for U-Val. As ν_R is reduced and passes through the various $n = 1$ and $n = 2$ R^2 conditions, the CO line moves upfield, then downfield (passing through the true isotropic chemical shift, as would be observed at natural abundance, near the exact R^2 condition), and back upfield, although not to its original chemical shift value. It is evident that the magnitude and MAS frequency range of the chemical shift variations depend on the strength of the dipole–dipole coupling between the R^2 partners, with the largest effect for the CO–Cα pair (2078 Hz coupling), and the smallest effect for the CO–Cγ1 pair. The linewidth and chemical shift changes are smaller for the $n = 2$ R^2 conditions.

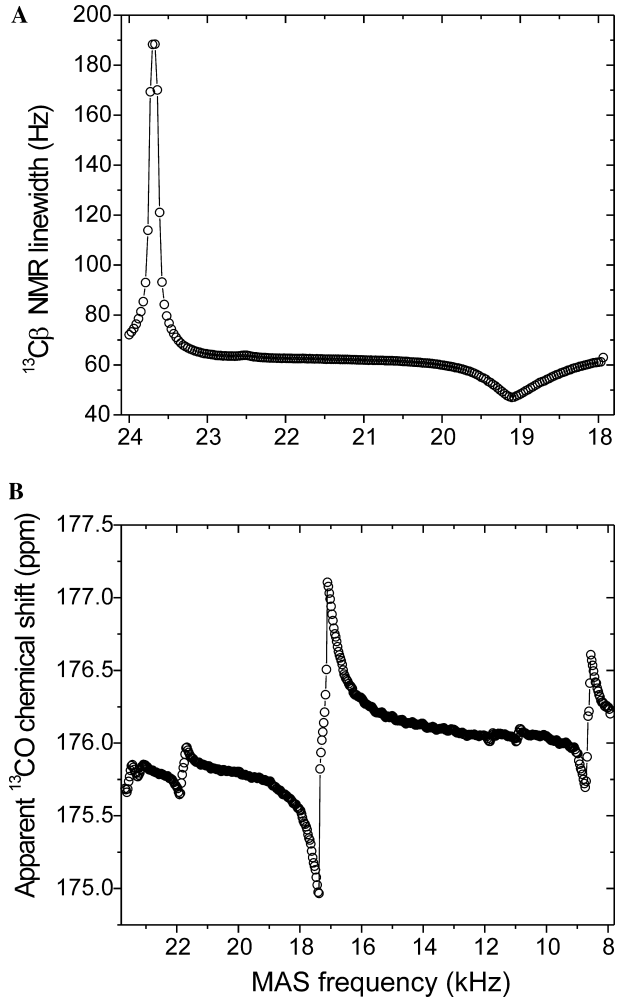

Fig. 4. (A) Dependence of the Cβ NMR linewidth in U-Ala on MAS frequency. Rotational resonance with the CO line occurs at 23.67 kHz. Rotational resonance between the CO and Cα lines occurs at 19.11 kHz, producing a narrowing of the Cβ line through *J*-decoupling. (B) Dependence of the apparent CO chemical shift in U-Val on MAS frequency. As the MAS frequency is lowered through the $n = 1$ rotational resonance conditions with Cγ2, Cγ1, Cβ, and Cα, and the $n = 2$ rotational resonance condition with Cα, pronounced upfield and downfield shifts occur. Linewidths (full width at half maximum) and apparent chemical shifts were determined from experimental spectra by fitting the ^{13}C NMR lines to Gaussian lineshapes.

The same phenomena are observed in non-crystalline systems such as amyloid fibrils. Fig. 5 shows a stack plot of the aliphatic regions of 1D CP/MAS spectra of VFFA-Aβ_{11-25} fibrils as ν_R is lowered to allow for the passage of the CO and Cα carbons of all labeled residues through R^2 conditions, and for the passage of the

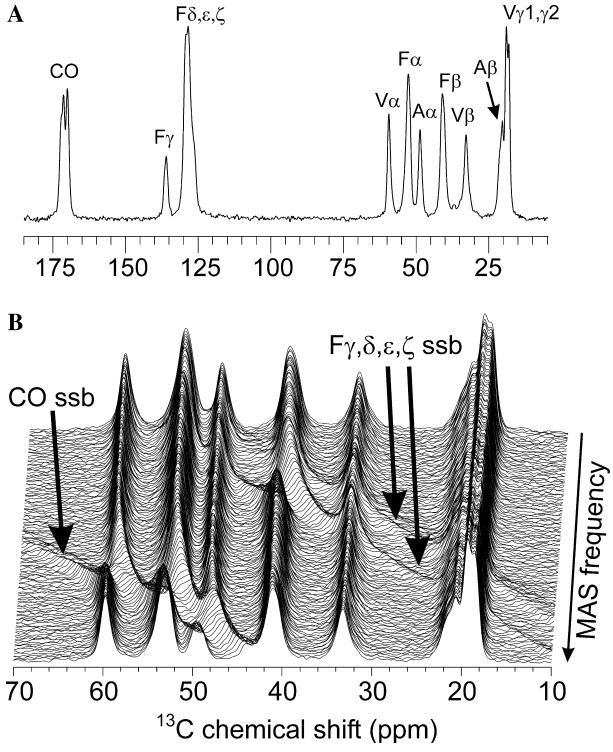

Fig. 5. (A) ^{13}C NMR spectrum of amyloid fibrils formed by VFFA-Aβ_{11-25}. Resonance assignments to uniformly labeled V18, F19, F20, and A21 residues are indicated. ^{13}C NMR lines from F19 and F20 are unresolved. (B) Stack plot representation of the dependence of the aliphatic region of the ^{13}C NMR spectrum on MAS frequency.

F19/F20 aromatic and Cβ carbons through the R^2 condition. Variations in the apparent Cα and F19/F20 Cβ chemical shifts as ν_R passes through the relevant R^2 conditions are clearly seen. Small but detectable reductions in the Cβ linewidths are seen near the CO/Cα R^2 conditions, attributable to *J*-decoupling.

3.2. ^{13}C–^{13}C distance measurements

In structural studies of biochemical systems such as amyloid fibrils, we are particularly interested in measuring relatively long ^{13}C–^{13}C distances, corresponding to relatively weak ^{13}C–^{13}C dipole–dipole couplings that produce relatively small effects on the NMR linewidths, even at R^2. These distance measurements may be carried out with R^2 polarization transfer experiments, using the pulse sequence in Fig. 1B. Fig. 6 shows the experimental dependence on τ_{RR} of the difference between Cγ2 and CO peak areas in spectra of U-Val at R^2, after selective inversion of CO magnetization (i.e., I_z–S_z decay curves). Simulated curves for a two-spin system are also shown, both for the best-fit ^{13}C–^{13}C distance (2.81 Å) and for the crystallographic CO–Cγ2 distances (sum of curves for 2.983 and 2.899 Å distances, for the two inequivalent molecules in the unit cell [32]). The difference between best-fit and crystallographic distances in Fig. 6 is quite similar to that reported previously for uniformly labeled L-threonine by Williamson et al. [21].

Experimentally determined single-quantum T_2 relaxation times for CO and Cγ2 in U-Val were 4.8 and 8.4 ms, respectively. The average relaxation rate $T_2^{-1} = (6.1\,\text{ms})^{-1}$ determined from these values was used in the 2.81 Å simulations in Fig. 6. The good agreement between the damping of oscillations in the experimental and simulated I_z–S_z decay curves provides support for the treatment of T_2 effects in our simulations (see Section 2), and for the implicit assumption that the fluctuating interactions that lead to T_2 relaxation of the CO and Cγ2 spins are uncorrelated. In order to achieve agreement between the values of the experimental and simulated curves at large τ_{RR}, a constant equal to 14.4% of the initial difference signal was subtracted from the simulated curve. Remaining deviations between experimental and simulated I_z–S_z values at large τ_{RR} may be due to intermolecular dipole–dipole couplings or residual intramolecular couplings to other ^{13}C spins away from R^2. Williamson et al. [21] also found that vertical offsets were required to achieve quantitative agreement between experimental and simulated I_z–S_z decay curves.

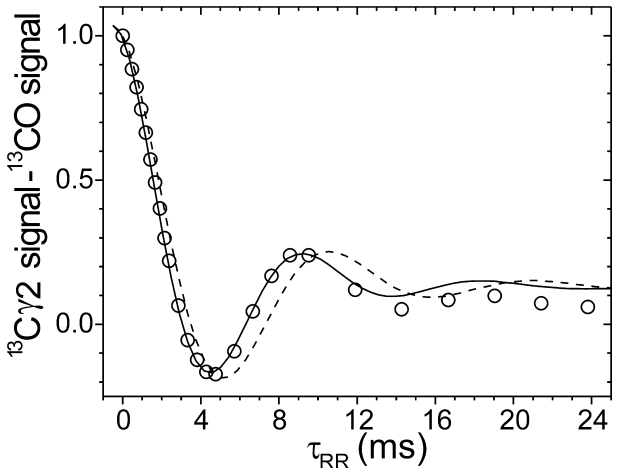

Fig. 6. Polarization transfer in U-Val at rotational resonance between the CO and Cγ2 lines. Experimental points (open circles) are the difference between Cγ2 and CO peak areas after selective inversion of the CO line, normalized to the difference at $\tau_{RR} = 0$. Simulations are shown for the CO–Cγ2 distances in the U-Val crystal structure (dashed line, calculated with $T_2 = 7.5$ ms) and the best-fit CO-Cγ2 distance of 2.81 Å (solid line, calculated with $T_2 = 6.1$ ms). Both simulated curves are scaled by 1.21 and offset by −0.174 in the vertical direction to match the experimental points, and offset by −0.5 ms in the horizontal direction to account for the 1.0 ms value of τ_G in the experiments.

In amyloid fibrils such as those formed by the full-length, 40-residue β-amyloid peptide ($A\beta_{1-40}$), hydrophobic sidechain–sidechain interactions stabilize contacts between non-hydrogen-bonded β-strands. According to our recent model for the $A\beta_{1-40}$ fibril structure [4], aromatic sidechains of phenylalanine residues may be of particular importance. Due to the favorable chemical shift separation of ^{13}C aromatic signals from CO and aliphatic ^{13}C signals, it is fairly straightforward to invert the aromatic ^{13}C lines of phenylalanine sidechains and, at readily achievable MAS frequencies, search for dipole–dipole couplings to aliphatic carbons of other sidechains, especially methyl carbons, at $n = 1$ R^2 conditions. Identification of intermolecular and nonsequential intramolecular aromatic/aliphatic contacts can provide important new constraints on molecular conformation and supramolecular structure.

In the less complex structure of VFFA-$A\beta_{11-25}$ fibrils at pH 7.4, extended antiparallel β-sheets that contain the central hydrophobic segment (i.e., residues 17–21) form the hydrogen bonded core of the fibrils [28,33]. In our sample with uniform labeling of residues 18–21, we expect intramolecular couplings between F19 and A21 sidechains and F20 and V18 sidechains, given the characteristic alternation of sidechain positions above and below the plane formed by the backbone atoms in β-sheets, with ^{13}C–^{13}C distances that depend on the sidechain conformations. Next-nearest-neighbor Cα–Cα distances within a β-strand peptide segment are typically 6.8–7.0 Å, but sidechain–sidechain ^{13}C–^{13}C distances can be considerably shorter. We also expect intermolecular couplings between F19 and V18 sidechains within a single antiparallel β-sheet, given the hydrogen-bonding registry established by earlier solid state NMR measurements on $A\beta_{11-25}$ fibrils formed at, pH 7.4 [28,33]. Sidechain–sidechain ^{13}C–^{13}C distances can be less than 4 Å for interstrand pairs in β-sheets. Additional

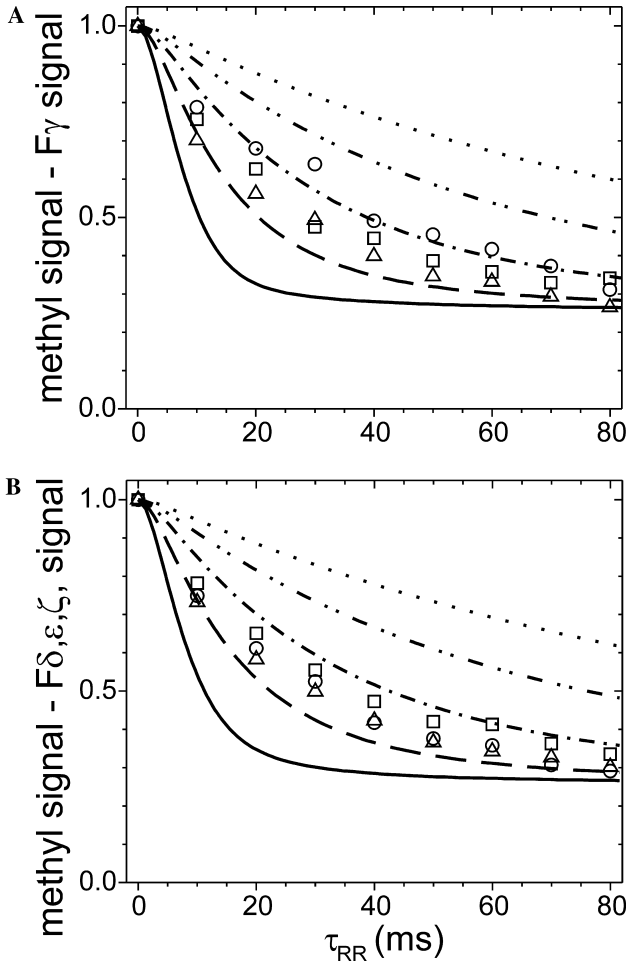

Fig. 7. Polarization transfer in VFFA-Aβ_{11-25} amyloid fibrils. (A) Difference between methyl and F19/F20 Cγ peak areas at rotational resonance for Cβ of A21 (circles), Cγ1 of V18 (triangles), and Cγ2 of V18 (squares). Simulated curves are for internuclear distances of 4.0 Å (solid line) to 6.0 Å (dotted line) in 0.5 Å increments, calculated with $T_2 = 4.82$ ms. (B) Difference between methyl and F19/F20 Cδ, Cε, Cζ (unresolved) peak areas at rotational resonance for Cβ of A21 (circles), Cγ1 of V18 (triangles), and Cγ2 of V18 (squares). Simulations as in part (A), but calculated with $T_2 = 4.41$ ms.

intermolecular couplings arising from contacts between different β-sheet layers are also possible.

Fig. 7A shows experimental I_z–S_z decay curves for VFFA-Aβ_{11-25} fibrils recorded at R^2 conditions between the Cγ line of F19 and F20 (unresolved, at 136.6 ppm) and the Cβ line of A21 (at 20.8 ppm), the Cγ1 line of V18 (at 19.5 ppm), and the Cγ2 line of V18 (at 18.6 ppm). Fig. 7B shows I_z–S_z decay curves at R^2 conditions between the center of the line containing Cδ, Cε, and Cζ signals of F19 and F20 (centered at 129 ppm) and the same methyl lines of A21 and V18. Figs. 7A and B also show simulated curves for ^{13}C–^{13}C distances from 4.0 to 6.0 Å, calculated with average T_2 relaxation rates determined from the measured T_2 values for the individual ^{13}C NMR lines (3.4, 3.0, and 8.2 ms for F19/F20 Cγ, other F19/F20 aromatic carbons, and methyl carbons, respectively). For all R^2 pairs in Fig. 7, the ^{13}C–^{13}C distances estimated by visual comparison of the experimental and simulated I_z–S_z decay curves are in the 4.5–5.5 Å range. Distances in this range are quite plausible, in light of the considerations discussed above and as confirmed by examination of model amyloid fibril structures [4].

Experimental decay curves in Fig. 7 were offset vertically by between 9 and −18% of the values at $\tau_{RR} = 0$ to optimize the agreement with simulated curves. The interpretation of these data is necessarily qualitative because of a number of uncertainties. For example, we do not know whether the Cγ sites of both F19 and F20 have similar couplings to a given methyl site, or whether only one of the Cγ sites has a significant coupling. Similarly, we do not know which of the F19 and F20 Cδ, Cε, and Cζ sites are most strongly coupled to a given methyl site. Nonetheless, measurements of the type shown in Fig. 7 are useful in high-molecular-weight systems with multiple uniformly labeled residues because they do establish close spatial proximity of particular aromatic and methyl sidechains. This is a strong constraint on tertiary structure.

3.3. Difference spectroscopy and relayed rotational resonance

In structural studies of systems with greater complexity and higher molecular weight, it may prove valuable to obtain indications of sidechain-sidechain contacts (or possibly backbone–sidechain contacts) by scanning ν_R over the possible R^2 conditions for a fixed and relatively large value of τ_{RR}, even without attempting to make quantitative determinations of internuclear distances. This can be done by recording a series of 1D difference spectra with the pulse sequence in Fig. 1B, subtracting spectra obtained with the selective inversion pulse on-resonance with the S_z line from spectra obtained with the selective inversion pulse off-resonance with all NMR lines, all other conditions being identical. Fig. 8 shows a stack plot of such difference spectra for VFFA-Aβ_{11-25} fibrils, obtained with inversion of F19/F20 aromatic signals and with ν_R values in a range that covers R^2 conditions with the F19/F20 Cβ line, the A21 Cβ line, and the V18 Cβ, and Cγ lines. Spinning sidebands of the F19/F20 aromatic signals appear in the difference spectra at all values of ν_R. As the relatively weakly coupled, inter-residue R^2 conditions are approached, the spinning sidebands appear to increase in intensity, reaching local maxima at the exact R^2 conditions. In a structurally complex system with multiple uniformly labeled residues, the locations of these maxima may be used to identify aliphatic carbons that are within a certain approximate radius (dependent on τ_{RR}) of the carbon sites whose signals are inverted by the Gaussian pulse in Fig. 1B. As the more strongly coupled,

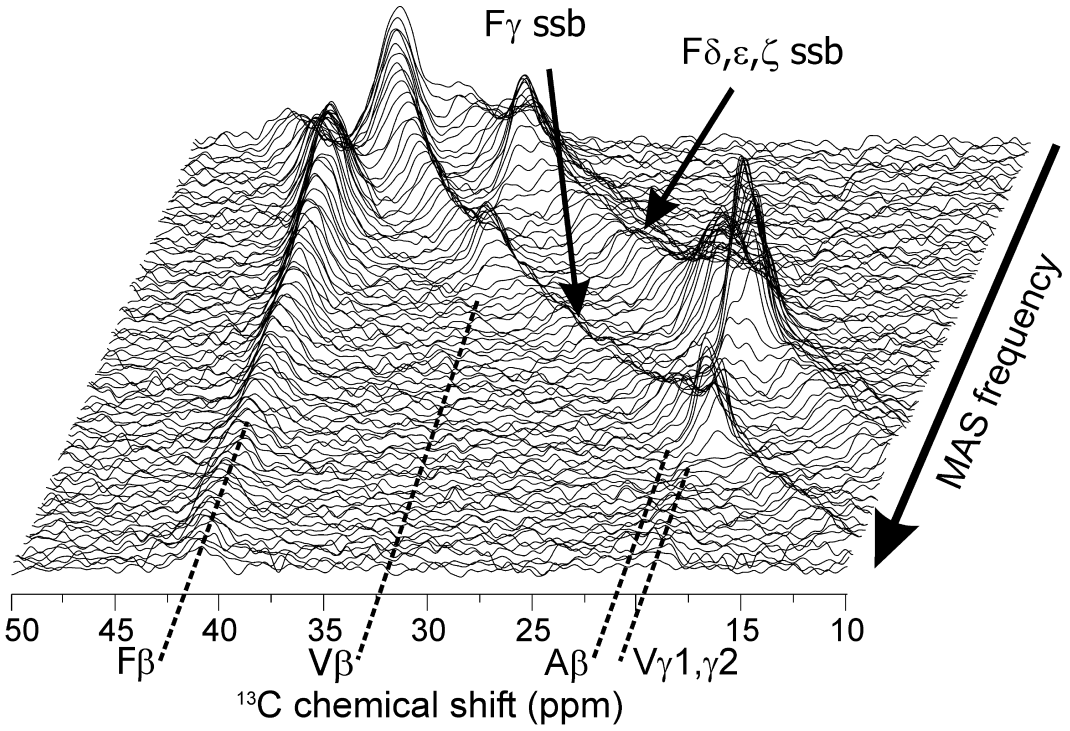

Fig. 8. Stack plot representation of the dependence of the rotational resonance difference spectrum of VFFA-Aβ_{11-25} fibrils on MAS frequency. The aliphatic region of the ^{13}C NMR spectrum is shown. Near rotational resonance with aliphatic ^{13}C lines of V18 and A21, the spinning sidebands of F19/F20 aromatic lines apparently increase in intensity in the difference spectrum. Spectra obtained with $\tau_{RR} = 80.0$ ms.

intra-residue R^2 conditions involving the F19/F20 Cβ line are approached in Fig. 8, the aromatic sidebands broaden into dipolar powder patterns with lineshapes that depend on the offset from the exact R^2 conditions.

In samples with a large number of uniformly labeled residues, spectral congestion may prevent the unambiguous assignment of R^2 conditions to individual carbon sites. For example, the methyl region of the 1D ^{13}C MAS spectrum may contain many overlapping signals, complicating the interpretation of aromatic/methyl R^2 data even at a qualitative structural level and even when only one aromatic sidechain is labeled. To overcome ambiguities arising from spectral congestion, it may then be useful to transfer ^{13}C polarization after R^2 exchange to other aliphatic carbons in a better-resolved region of the MAS spectrum before signal detection. As an illustration of this relayed R^2 approach, Fig. 9 shows experimental data for U-Val at the CO/Cγ2 R^2 condition, obtained with the pulse sequence in Fig. 1C and with $\tau_{RR} = 61.2$ ms. Peak areas in the difference spectrum (with and without selective inversion of the CO line) are plotted as functions of τ_{SD}. As τ_{SD} increases, the Cβ and Cγ1 lines increase in intensity due to ^{13}C–^{13}C spin diffusion from Cγ2 or CO.

In future experiments, band-selective ^{13}C–^{13}C recoupling sequences may be used to control polarization transfer pathways and optimize the sensitivity of relayed R^2. In some circumstances, it may prove useful to place τ_{SD} (the relay period) before τ_{RR} (the R^2 period). For example, one could selectively invert the resolved Cα line of a given uniformly labeled residue, transfer polarization to the unresolved CO line of the same res-

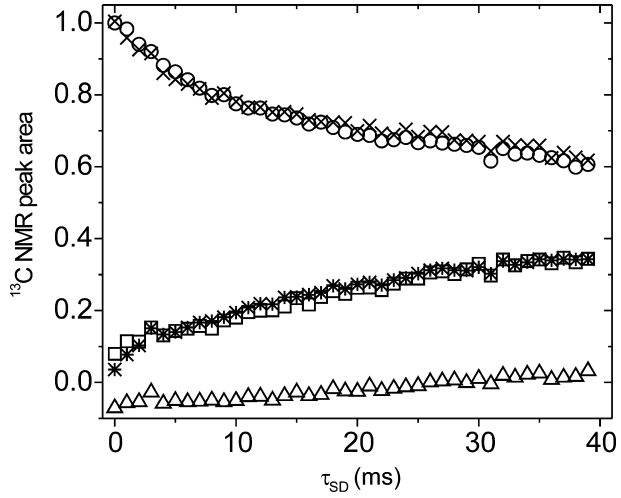

Fig. 9. Relayed rotational resonance data for U-Val, obtained at rotational resonance between the CO and Cγ2 lines and with $\tau_{RR} = 61.2$ ms. Peak areas in the rotational resonance difference spectrum are plotted for the CO (circles), Cα (triangles), Cβ (squares), Cγ1 (stars), and Cγ2 (crosses) lines, normalized to the CO peak area at $\tau_{SD} = 0$. With increasing τ_{SD}, NMR lines of sites that are not on rotational resonance, but are coupled to a site on rotational resonance, grow in intensity. (Initial Cα area in the difference spectrum is negative because a sideband of the Cα line was irradiated by the Gaussian-shaped π pulse in the off-resonance scans.)

idue in a relatively short τ_{SD} period, and then look for inter-residue R^2 exchange to methyl carbons of other uniformly labeled residues.

4. Conclusions

We have shown how the R^2 recoupling effect, originally applied as a structural tool in studies of samples prepared with pairs of isotopic labels, can be used to make quantitative and semi-quantitative structural measurements on biomolecular samples with uniformly ^{13}C-labeled segments or components. The main requirement for the applicability of R^2 as a tool for long-range distance measurements is that the 1D MAS spectrum be sufficiently well resolved that selective inversion of at least one resonance of interest and detection and assignment of other resonances of interest are possible. Relayed R^2 measurements, introduced above, can alleviate complications arising from unresolved resonances. In some cases, ambiguities arising from spectral overlap can also be eliminated on the basis of prior knowledge about the molecular structure or amino acid sequence. We have also demonstrated two effects that may be important in the design and interpretation of R^2 measurements and other measurements on uniformly labeled samples, namely J-decoupling at R^2 conditions and the dependence of apparent ^{13}C chemical shifts on MAS frequency in the vicinity of (but persisting far from) R^2 conditions. Together with the work of Williamson et al. [21] and others [22–25], the results presented above set the stage for applications of R^2 in future structural studies of peptides and proteins with uniformly labeled residues, as well as other uniformly labeled systems.

Acknowledgments

We thank Dr. Nathan Oyler for the recrystallization of U-Val, Dr. Gerd Buntkowsky for assisting with the preparation of the $A\beta_{11–25}$ fibrils, and Dr. Lewis Pannell for mass spectrometry of the $A\beta_{11–25}$ samples. This work was supported in part by a grant from the Intramural AIDS Targeted Antiviral Program of the National Institutes of Health.

References

[1] F. Castellani, B. van Rossum, A. Diehl, M. Schubert, K. Rehbein, H. Oschkinat, Structure of a protein determined by solid-state magic-angle-spinning NMR spectroscopy, Nature 420 (2002) 98–102.

[2] C.M. Rienstra, L. Tucker-Kellogg, C.P. Jaroniec, M. Hohwy, B. Reif, M.T. McMahon, B. Tidor, T. Lozano-Perez, R.G. Griffin, De novo determination of peptide structure with solid-state magic-angle spinning NMR spectroscopy, Proc. Natl. Acad. Sci. USA 99 (2002) 10260–10265.

[3] C.P. Jaroniec, C.E. MacPhee, N.S. Astrof, C.M. Dobson, R.G. Griffin, Molecular conformation of a peptide fragment of transthyretin in an amyloid fibril, Proc. Natl. Acad. Sci. USA 99 (2002) 16748–16753.

[4] A.T. Petkova, Y. Ishii, J.J. Balbach, O.N. Antzutkin, R.D. Leapman, F. Delaglio, R. Tycko, A structural model for Alzheimer's β-amyloid fibrils based on experimental constraints from solid state NMR, Proc. Natl. Acad. Sci. USA 99 (2002) 16742–16747.

[5] J. Pauli, M. Baldus, B. van Rossum, H. de Groot, H. Oschkinat, Backbone and side-chain ^{13}C and ^{15}N signal assignments of the alpha-spectrin SH3 domain by magic angle spinning solid-state NMR at 17.6 Tesla, Chembiochem 2 (2001) 272–281.

[6] A. McDermott, T. Polenova, A. Bockmann, K.W. Zilm, E.K. Paulsen, R.W. Martin, G.T. Montelione, Partial NMR assignments for uniformly (^{13}C,^{15}N)-enriched BPTI in the solid state, J. Biomol. NMR 16 (2000) 209–219.

[7] K. Nomura, K. Takegoshi, T. Terao, K. Uchida, M. Kainosho, Determination of the complete structure of a uniformly labeled molecule by rotational resonance solid-state NMR in the tilted rotating frame, J. Am. Chem. Soc. 121 (1999) 4064–4065.

[8] M. Hong, K. Jakes, Selective and extensive ^{13}C labeling of a membrane protein for solid-state NMR investigations, J. Biomol. NMR 14 (1999) 71–74.

[9] A. Detken, E.H. Hardy, M. Ernst, M. Kainosho, T. Kawakami, S. Aimoto, B.H. Meier, Methods for sequential resonance assignment in solid, uniformly ^{13}C,^{15}N-labelled peptides: quantification and application to antamanide, J. Biomol. NMR 20 (2001) 203–221.

[10] S.K. Straus, T. Bremi, R.R. Ernst, Experiments and strategies for the assignment of fully ^{13}C/^{15}N-labelled polypeptides by solid state NMR, J. Biomol. NMR 12 (1998) 39–50.

[11] J.J. Balbach, Y. Ishii, O.N. Antzutkin, R.D. Leapman, N.W. Rizzo, F. Dyda, J. Reed, R. Tycko, Amyloid fibril formation by $A\beta_{16\text{-}22}$, a seven-residue fragment of the Alzheimer's β-amyloid peptide, and structural characterization by solid state NMR, Biochemistry 39 (2000) 13748–13759.

[12] Y. Ishii, ^{13}C–^{13}C dipolar recoupling under very fast magic angle spinning in solid-state nuclear magnetic resonance: applications to distance measurements, spectral assignments, and high-throughput secondary-structure determination, J. Chem. Phys. 114 (2001) 8473–8483.

[13] E.R. Andrew, S. Clough, L.F. Farnell, T.D. Gledhill, I. Roberts, Phys. Lett. 21 (1966) 505–506.

[14] D.P. Raleigh, G.S. Harbison, T.G. Neiss, J.E. Roberts, R.G. Griffin, Homonuclear J-couplings and rotationally induced sideband enhancements in NMR spectra of rotating solids, Chem. Phys. Lett. 138 (1987) 285–290.

[15] B.H. Meier, W.L. Earl, A double-quantum filter for rotating solids, J. Am. Chem. Soc. 109 (1987) 7937–7942.

[16] D.P. Raleigh, M.H. Levitt, R.G. Griffin, Rotational resonance in solid-state NMR, Chem. Phys. Lett. 146 (1988) 71–76.

[17] M.G. Colombo, B.H. Meier, R.R. Ernst, Rotor-driven spin diffusion in natural-abundance ^{13}C spin systems, Chem. Phys. Lett. 146 (1988) 189–196.

[18] Z.H. Gan, D.M. Grant, Pseudo-spin rotational resonance and homonuclear dipolar NMR of rotating solids, Mol. Phys. 67 (1989) 1419–1430.

[19] D.P. Raleigh, F. Creuzet, S.K.D. Gupta, M.H. Levitt, R.G. Griffin, Measurement of internuclear distances in polycrystalline solids: rotationally enhanced transfer of nuclear spin magnetization, J. Am. Chem. Soc. 111 (1989) 4502–4503.

[20] M.H. Levitt, D.P. Raleigh, F. Creuzet, R.G. Griffin, Theory and simulations of homonuclear spin pair systems in rotating solids, J. Chem. Phys. 92 (1990) 6347–6364.

[21] P.T.F. Williamson, A. Verhoeven, M. Ernst, B.H. Meier, Determination of internuclear distances in uniformly labeled molecules by rotational resonance solid-state NMR, J. Am. Chem. Soc. 125 (2003) 2718–2722.
[22] K. Nomura, K. Takegoshi, T. Terao, K. Uchida, M. Kainosho, Three-dimensional structure determination of a uniformly labeled molecule by frequency-selective dipolar recoupling under magic-angle spinning, J. Biomol. NMR 17 (2000) 111–123.
[23] S. Dusold, H. Maisel, A. Sebald, Magnitudes and orientations of interaction tensors determined from rotational resonance MAS NMR lineshapes of a four-^{13}C spin system, J. Magn. Reson. 141 (1999) 78–90.
[24] L. Duma, S. Hediger, A. Lesage, D. Sakellariou, L. Emsley, Carbon-13 lineshapes in solid-state NMR of labeled compounds. Effects of coherent CSA-dipolar cross-correlation, J. Magn. Reson. 162 (2003) 90–101.
[25] A. Samoson, T. Tuherm, J. Past, Rotation sweep NMR, Chem. Phys. Lett. 365 (2002) 292–299.
[26] T. Nakai, C.A. McDowell, Application of floquet theory to the nuclear magnetic resonance spectra of homonuclear 2-spin systems in rotating solids, J. Chem. Phys. 96 (1992) 3452–3466.
[27] A. Schmidt, S. Vega, The floquet theory of nuclear magnetic resonance spectroscopy of single spins and dipolar coupled spin pairs in rotating solids, J. Chem. Phys. 96 (1992) 2655–2680.
[28] A.T. Petkova, G. Buntkowsky, F. Dyda, R.D. Leapman, W.-M. Yau, R. Tycko, Solid state NMR reveals a pH-dependent antiparallel β-sheet registry in fibrils formed by a β-amyloid peptide, J. Mol. Biol. 335 (2004) 247–260.
[29] K. Takegoshi, S. Nakamura, T. Terao, ^{13}C–^{1}H dipolar-assisted rotational resonance in magic-angle spinning NMR, Chem. Phys. Lett. 344 (2001) 631–637.
[30] A.E. Bennett, C.M. Rienstra, M. Auger, K.V. Lakshmi, R.G. Griffin, Heteronuclear decoupling in rotating solids, J. Chem. Phys. 103 (1995) 6951–6958.
[31] T. Karlsson, M.H. Levitt, Longitudinal rotation resonance echoes in solid state nuclear magnetic resonance: investigation of zero quantum spin dynamics, J. Chem. Phys. 109 (1998) 5493–5507.
[32] B. Dalhus, C.H. Gorbitz, Crystal structures of hydrophobic amino acids. 1. redeterminations of L-methionine and L-valine at 120 K, Acta Chem. Scand. 50 (1996) 544–548.
[33] R. Tycko, Y. Ishii, Constraints on supramolecular structure in amyloid fibrils from two-dimensional solid-state NMR spectroscopy with uniform isotopic labeling, J. Am. Chem. Soc. 125 (2003) 6606–6607.